

IMPROVING PHOTOMETRIC REDSHIFTS USING GALEX OBSERVATIONS FOR THE SDSS STRIPE 82 AND THE NEXT GENERATION OF SZ CLUSTER SURVEYS

MICHAEL D. NIEMACK¹, RAUL JIMENEZ², LICIA VERDE², FELIPE MENANTEAU³, BEN PANTER⁴, DAVID SPERGEL⁵

Draft version November 18, 2018

ABSTRACT

Four large-area Sunyaev-Zeldovich (SZ) experiments – APEX-SZ, SPT, ACT, and Planck – promise to detect clusters of galaxies through the distortion of Cosmic Microwave Background photons by hot ($> 10^6$ K) cluster gas (the SZ effect) over thousands of square degrees. A large observational follow-up effort to obtain redshifts for these SZ-detected clusters is under way. Given the large area covered by these surveys, most of the redshifts will be obtained via the photometric redshift (photo- z) technique. Here we demonstrate, in an application using ~ 3000 SDSS stripe 82 galaxies with $r < 20$, how the addition of GALEX photometry (F_{UV} , N_{UV}) greatly improves the photometric redshifts of galaxies obtained with optical *griz* or *ugriz* photometry. In the case where large spectroscopic training sets are available, empirical neural-network-based techniques (e.g., ANNz) can yield a photo- z scatter of $\sigma_z = 0.018(1+z)$. If large spectroscopic training sets are not available, the addition of GALEX data makes possible the use simple maximum likelihood techniques, without resorting to Bayesian priors, and obtains $\sigma_z = 0.04(1+z)$, accuracy that approaches the accuracy obtained using spectroscopic training of neural networks on *ugriz* observations. This improvement is especially notable for blue galaxies. To achieve these results, we have developed a new set of high resolution spectral templates based on physical information about the star formation history of galaxies. We envision these templates to be useful for the next generation of photo- z applications. We make our spectral templates and new photo- z catalogs available to the community at www.ice.csic.es/personal/jimenez/PHOTOZ.

Subject headings: galaxies, clusters, photometric redshifts, SZ, dark energy, general

1. INTRODUCTION

Thousands of square degrees of the sky are currently being observed at mm wavelengths by three experiments: APEX-SZ⁶, South Pole Telescope (SPT)⁷ and Atacama Cosmology Telescope (ACT)⁸. In addition, the Planck satellite, to be launched this fall, will observe the whole sky. The promise of these surveys is to provide a nearly mass-selected galaxy cluster sample via the Sunyaev-Zeldovich (SZ) effect (Sunyaev & Zeldovich 1972). Because of the lack of sensitivity of the SZ-effect to redshift, clusters or groups of galaxies detected this way need follow-up observations at other wavelengths to determine their redshifts. The large area of sky covered and the large number of expected detections make spectroscopic follow-up of galaxies in every cluster prohibitive. Upcoming surveys will rely on redshifts obtained from broadband photometry (photometric redshifts or photo- z) or custom-designed narrow-band photometry (Moles et al. 2005; Benítez et al. 2008). As broadband photometry provides low resolution spectral information, the determination of galaxy-redshifts can be affected by relatively large errors. Photo- z errors can limit the accuracy of

cosmological studies using galaxies or clusters, which highlights the importance of improving photo- z determinations. For example, SPT and ACT will attempt to constrain the dark energy equation of state using SZ selected clusters and photo- z (Carlstrom et al. 2005). Lima & Hu (2007) calculate that a photo- z bias of 0.003 and scatter of 0.03 will cause a $\sim 10\%$ increase in the amplitude of the equation of state error bars achieved by SPT using this approach. The above surveys will require photo- z not only for SZ clusters but also for field galaxies, to carry out ancillary science such as exploiting the signal of CMB weak lensing (e.g., Carbone et al. 2007) by large scale structure and the kinetic-SZ effect (e.g., Hernández-Monteagudo et al. 2006): two powerful probes of the growth of structure, which are useful, for example, in distinguishing between modified gravity and dark energy as the source of the present accelerating expansion of the universe.

The use of broad-band photometry to determine redshifts is not new (see first attempts by Baum 1962 and Koo 1985). In its minimalistic approach it consists of simply finding the best fit redshift using a series of galaxy templates, which can be either chosen from stellar population models or empirically (Koo 1999) as long as the set is exhaustive (i.e. fully describes the galaxy population). With the arrival of large spectrographs, it became clear that a refinement of the above technique could be achieved by using small subsets of spectroscopic redshifts as “training sets” for larger photometric samples. One can then use these training sets as inputs for empirical fits to the magnitudes versus z (e.g. Budavári et al. 2005) or for artificial neural network codes to compute photo- z (Vanzella et al. 2004; Collister & Lahav 2004; Oyaizu et al. 2007). Another approach is to use prior in-

¹ Department of Physics, Jadwin Hall, Princeton University, Princeton, NJ 08544, USA; mniemack@princeton.edu

² Institute of Space Sciences (CSIC-IEEC)/ICREA, Campus UAB, Barcelona 08193, Spain; raul@ieec.uab.es

³ Department of Physics and Astronomy, Rutgers University, NJ, USA

⁴ SUPA, Institute for Astronomy, University of Edinburgh, Royal Observatory, Edinburgh EH9-3HJ, UK

⁵ Department of Astrophysical Sciences, Peyton Hall, Princeton University, Princeton, NJ 08544, USA

⁶ www.apex-telescope.org

⁷ spt.uchicago.edu

⁸ www.physics.princeton.edu/act

formation about galaxies, like the fact that faint galaxies tend to be farther away, as a Bayesian prior for computing the redshift likelihood from the templates (Benítez 2000; Ilbert et al. 2006; Feldmann et al. 2006). Other recently developed techniques that go beyond simple photometry fits include using structural properties of galaxies like their size or surface brightness to obtain more accurate photo- z (e.g., Wray & Gunn 2007).

The above methods have their pros and cons. For example, methods based on training sets, because of their empirical basis, can only be reliably extended as far as the spectroscopic redshift limit. Training sets for surveys such as the dark energy survey (DES) and the Large Synoptic Survey Telescope (LSST) survey will need of the order of hundreds of thousands of spectroscopic redshifts (Connolly et al. 1997; Oyaizu et al. 2006).

To use Bayesian prior-based methods, one needs to construct and test different priors for different redshift ranges and surveys, which also requires spectroscopic redshifts to accurately generate the prior distributions.

Given the need to obtain relatively accurate photo- z for the large SZ survey areas we have explored an alternative approach. The goal of this approach is to optimize photo- z accuracy while minimizing external assumptions (priors) and additional data acquisition.

Our approach, presented in detail below, consists of obtaining moderate depth observations with the Galaxy Evolution Explorer (GALEX) combined with optical *griz* data. This data combination was first tried by Budavári et al. (2005), Way & Srivastava (2006), and Ball et al. (2007), who used empirical approaches with spectroscopic training sets for photo- z determination. Adding the two GALEX broad bands at central wavelengths of ~ 1500 Å (F_{UV}) and ~ 2300 Å (N_{UV}) to optical *griz* photometry, improves photo- z determinations, while requiring minimal assumptions about external priors, for the following reason. The 4000 Å break, which is the most commonly used spectral feature for optical photo- z determination, is greatly reduced for blue galaxies, making it more difficult to use as a redshift indicator. This problem is particularly acute at $z \gtrsim 0.5$, where most galaxies are young and have high star formation rates (e.g., Heavens et al. 2004). The 912 Å Lyman-limit, on the other hand, is exhibited by all galaxies (Fig. 2). Filters that sample closer to the Lyman-limit help to pin down the galaxy type and redshift, especially for blue galaxies with no substantial 4000 Å break. Further, given the strong sensitivity of the *UV* to star formation, one can directly obtain a measure of star formation.

In carrying out this work, we found that galaxy templates with well motivated blue spectra (in particular, blue-wards of 3000 Å) are not publicly available. Either this region of the spectrum was missing (like in the original Coleman, Wu, & Weedman 1980 templates) or it was modeled roughly with no spectral features beyond the Lyman-limit. Motivated by the need to provide reliable empirical templates in this region of the spectrum and higher spectral resolution than currently available models, we have developed our own templates. To do so we have exploited our knowledge of the star formation history of galaxies over cosmic time (Panter et al. 2007) to help us build physically motivated templates.

We present a test of the performance of this approach

on spectroscopic samples from the Sloan Digital Sky Survey (SDSS) stripe 82 region. We find that, in the case where large spectroscopic training sets are available, empirical neural-network-based techniques (e.g., ANNz Collister & Lahav 2004; Oyaizu et al. 2007) give a $\sigma_z = 0.018(1+z)$ for optical photometry combined with GALEX observations. If large spectroscopic training sets are not available, the addition of GALEX data make possible the use of simple maximum likelihood techniques, without resorting to Bayesian priors, and obtains $\sigma_z = 0.04(1+z)$, which approaches the accuracy obtained using spectroscopic training of neural networks on *ugriz* observations. In particular, we show how the large number of catastrophic failures that occur for *griz*-based and *ugriz*-based maximum likelihood photometric redshift determinations is nearly eliminated by adding UV photometry from GALEX data. The improvement is especially notable for blue galaxies with $g-r < 0.6$, for which photo- z scatter of $0.03(1+z)$ is achieved on galaxies with $r < 19$ and $z \lesssim 0.25$. As noted below and by Ilbert et al. (2006), the absence of the *u* band significantly degrades the performance of the photo- z estimation. We show that the addition of GALEX *UV* observations is preferable to the addition of optical *u* band observations.

The rest of the paper is organized as follows: in §2 we describe our source sample. In §3 we present our method and details of the implementation. In §4 we discuss our results. Conclusions are presented in §5.

2. SOURCE SAMPLE

Our GALEX observations comprise a Legacy program awarded in cycle 3, with the goal of mapping ~ 100 deg² with 3 ks exposure time per pointing in both the F_{UV} and N_{UV} filters. We chose to map roughly 11 deg² covering the Blanco Cosmology Survey⁹ (BCS) 23-hour field at declination -55° and a larger area of the equatorial stripe 82, which is covered by SDSS. Both areas have *griz* observations, and SDSS also has *u* observations. The BCS field is part of the common SZ area survey; however, as there is currently no significant sample of spectroscopic redshifts in the BCS region to validate our photo- z , BCS analysis will not be presented here. The SDSS stripe 82 has been observed by ACT and (of course) offers a sample of SDSS spectroscopic redshifts to test the photo- z performance. We took advantage of the fact that the stripe 82 survey area includes a number of the GALEX Medium Imaging Survey (MIS) fields, which already had many > 1.5 ks observations and therefore needed only partial additional observations to reach our 3 ks target. In total we will collect ~ 210 ks of integration time — merely 2.4 days of observations.

At the time this analysis was completed, only about half of the planned observations had been made. The stripe 82 data set used for this analysis is comprised of 56 GALEX fields (~ 55 deg² of coverage, although some field edges lie outside the SDSS stripe 82 region) to N_{UV} depths between 2 ks and 6.5 ks (Fig. 1). These depths allow us to probe deeper magnitudes and a more complete sample than has been possible with previous photo- z studies that used GALEX data (Budavári et al. 2005; Way & Srivastava 2006; Ball et al. 2007). Of those

⁹ cosmology.uiuc.edu/BCS

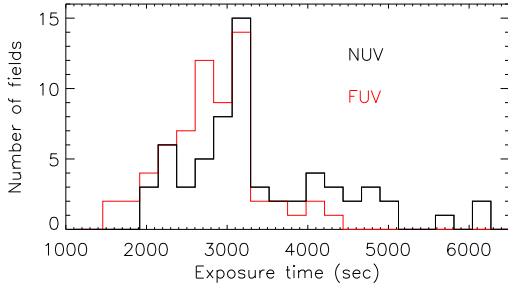


FIG. 1.— Distribution of exposure times on the GALEX fields used in this analysis for N_{UV} (black) and F_{UV} (red) observations. Fields were only used with N_{UV} exposure > 2 ks.

fields, 41 are publicly available MIS data, and the other 15 are from our guest investigator proposal.¹⁰

2.1. Magnitudes

Accurate photometry is critical for obtaining accurate photo- z . Because of the differences in the point spread functions (PSF) of different instruments and between bands, simple aperture photometry is not appropriate for this study. The SDSS PSF widths are approximately $1.5''$ and vary with sky brightness (Abazajian et al. 2003), while GALEX PSF widths vary across the field between roughly $4''$ and $7''$ (Morrissey et al. 2005). Our approach is to use AB magnitude measures that are as close as possible to the total flux emitted by the galaxy in each band.

As part of the standard GALEX pipeline for each field, SExtractor is run on both the F_{UV} and N_{UV} images¹¹ to extract multi-pixel sources that are detected above the noise threshold in background-subtracted images (Bertin & Arnouts 1996). We use the N_{UV} and F_{UV} *mag_auto* outputs of SExtractor, which optimizes elliptical apertures for each source to integrate the total flux. The F_{UV} bandwidth and transmission are both roughly a factor of two smaller than the N_{UV} (Figure 2), causing it to have substantially lower sensitivity. Because of this, far fewer sources are independently detected in the F_{UV} band.

For the SDSS data we explored the use of both *C-model* and *model* magnitude measurements. These magnitudes consist of fitting models to the profile of the galaxy composed of an exponential disc and a deVaucouleurs profile. The fits are integrated to three and seven times the characteristic radius respectively, at which point the function is truncated to smoothly go to zero within one additional characteristic radius. For the *model* magnitudes all bands are measured using the best fit model to the r -band data, while for the *C-model* magnitudes, the two fits are weighted based on the quality of the fit and combined to obtain the best fitting profile for each filter band.¹² The *C-model* measurement provides the best estimate of the total photometric flux for each SDSS band.¹³ While testing the template-fitting photo- z tech-

niques (§3.2) we found that *model* magnitudes provide a better relative calibration when comparing only SDSS bands (especially after adding the Padmanabhan et al. (2007) “ubercalibration” corrections); however, the *C-model* magnitudes provide a better absolute calibration for comparing with other instruments, such as GALEX. Both *model* and *C-model* magnitudes were also tested using the ANNz analysis described in §3.3, and no significant differences were found between the results using the different magnitudes. The ANNz results presented in §4.2 were calculated using *model* magnitudes.

Magnitude corrections of -0.04 and $+0.02$ are applied to the SDSS u and z bands respectively to convert from SDSS magnitudes into AB magnitudes.¹⁴ All reported magnitudes are in the AB system. In §4 we assess the performance of our photo- z analysis on those SDSS galaxies with spectroscopic redshifts with confidence > 0.9 . SDSS objects are excluded from the catalog using the “blended,” “nodeblend,” and “saturated” flags. The majority of the SDSS spectroscopic measurements have $r < 18$, although, there are also a substantial number of spectroscopic measurements between $18 < r < 20$ (which are primarily Luminous Red Galaxies), so we have limited our current analysis to the $r < 20$ magnitude regime (except as discussed in Fig. 8 and §4.3).

We emphasize that by using total magnitudes for each band we minimize the potential problem of missing light because of choosing an aperture in one band that does not encompass all the light in other bands. Measuring the total light is important when using the GALEX bands both because of the different PSF sizes and because most of the star formation in galaxies takes place at the galaxy perimeter; thus, a fixed aperture based on a single optical band can exclude much of the light from recent star formation, which is measured by the UV bands.

2.2. Catalog matching

The GALEX and optical catalogs are merged as follows: we initially assign optical sources to a GALEX field pointing if they fall within $35.1'$ of the GALEX field center. This cuts the noisiest region of the GALEX fields (near the edges), while maintaining complete sky coverage between neighboring fields (i.e. leaving no gaps). Within every GALEX field, each optical source is matched to the nearest GALEX object with a N_{UV} detection within a $4''$ radius, which is a relatively conservative matching radius (Agüeros et al. 2005). After all sources in the field are assigned, the combined catalog is searched to test whether any two optical sources are assigned to the same GALEX object. When there are overlapping assignments, the closest source to the GALEX position is selected and the other is removed from the catalog.¹⁵ Sources that do not have a GALEX detection or overlapping assignments are kept in the catalog for spectroscopic confirmation tests. We characterize the distributions of GALEX F_{UV} and N_{UV} magnitudes in each field using histograms with 0.1 magnitude bins. The magnitude limit used for other sources in the

¹⁰ Niemack (2008) describes the source sample in more detail.

¹¹ galex.stsci.edu/GR2/?page=ddfaq#2

¹² www.sdss.org/dr5/algorithms/photometry.html

¹³ While it may not be the case for low signal-to-noise cases, in the high signal-to-noise regime this procedure yields the total photometric flux and is not affected by systematic errors. For the objects considered the SDSS signal-to-noise is > 5 .

¹⁴ www.sdss.org/dr6/algorithms/fluxcal.html#sdss2ab

¹⁵ Removing sources with overlapping assignments was also explored and had negligible impact on the results in this paper since so few sources had overlapping assignments.

same field during photo- z analysis is set to be the highest magnitude where the number of galaxies exceeds half of the number at the peak magnitude bin (Niemack 2008). Sources with magnitudes higher than this limit (as well as objects with no N_{UV} detection) are labeled as non-detections, and this magnitude limit is used for the non-detections in the photo- z calculation (§3).

In 56 GALEX fields in stripe 82, ~ 3000 SDSS sources with spectroscopic redshifts were found that meet the above criteria. Of these sources, 75% were found to have N_{UV} detections within the $4''$ matching radius, and only two pairs of them were matched to the same GALEX source. Only seven of the sources had $r > 20$, which we treat as the magnitude limit of the spectroscopic analysis. When generating the photo- z catalogs, we also use SDSS objects without spectroscopic data. In the same 56 GALEX fields almost 150,000 SDSS sources were found with magnitude $r < 21$, and 55% of those were successfully matched to GALEX sources. Less than 1% of those were excluded because they were matched to the same GALEX source as another optical source. Both catalogs were also searched for SDSS sources with multiple GALEX sources within a $4''$ radius, and none were found in the spectroscopic catalog, while nine were found in the photometric sample and were removed from the catalog.

3. METHODS

After adding the GALEX bands, we consider two different approaches for computing the photo- z . First we describe a spectral energy distribution (SED, or template-based) photo- z calculation technique and the new SED templates that we have developed. This approach assumes no prior knowledge of the redshift distribution and does not require spectroscopic measurements. Our second approach is to analyze the same GALEX plus optical catalog using ANNz techniques to train the photo- z calculation with the SDSS spectroscopic measurements.

To quantify the accuracy of different photo- z analyses, we define the redshift error as

$$dz \equiv \frac{(z_{ph} - z_{sp})}{(1 + z_{sp})}, \quad (1)$$

where z_{ph} is the photo- z and z_{sp} is the spectroscopic z . The mean, z^{bias} , and standard deviation, σ_z , of dz (i.e. the photo- z bias and scatter) are calculated for all galaxies with $z_{ph} < 1$, which is motivated by the fact that given the optical and UV depths, we do not expect to detect galaxies near or above $z = 1$. In the SDSS results presented, these $z > 1$ failures amount to less than 1% of the galaxies in the spectroscopic catalog and $\sim 1\%$ of the GALEX detected galaxies with $r < 20$ in the photometric catalog. A final cut is made on objects with $N_{UV} - g > 1$ as this color is typical of QSO's rather than galaxies. This cut also removes less than 1% of the complete SDSS spectroscopic catalog and $\sim 3\%$ of the GALEX detected galaxies with $r < 20$ in the photometric catalog.

The analysis is done on different combinations of the seven optical (SDSS) and UV bands. This allows us to study the impact of including different bands on photo- z accuracy and thus estimate the importance of different bands for future observations. Our photo- z are then compared to the recently published results of the SDSS ANNz

photo- z pipeline (henceforth ANNz; Oyaizu et al. 2007), which was developed using a spectroscopic training and validation set comprised of $\sim 640,000$ galaxies (Fig. 3).

We note that when reporting standard deviations to study the performance of the photo- z we have *not* excluded outliers (with the exception of cutting the small number of galaxies with $z > 1$). Excluding or down-weighting outliers is common practice in the photo- z literature, motivated by the fact that the photo- z error distribution often is a Gaussian around the peak but has long tails. As we quote standard deviations with the outliers included, caution is needed when comparing our numbers with those in the literature. In particular, for the maximum likelihood analysis presented in Fig. 3, the standard down-weighting of the outliers would reduce the *ugriz* photo- z scatter by 20% and the GALEX + *griz* photo- z scatter by 15%, while having a much smaller effect on the SDSS ANNz performance.

3.1. New spectral templates for photo- z

For template-based photo- z calculation, we need a basis of spectral templates that represents galaxies in the redshift range of interest and for the magnitude range of the catalog. The approach in the literature so far has been to either use empirical templates (Coleman, Wu, & Weedman 1980; Kinney et al. 1996) or use synthetic models with simple recipes to model the star formation law in galaxies, most typically using a declining exponential.

Recent advances in both observations and stellar modeling have allowed different groups to determine the complete star formation history of galaxies (Heavens et al. 2004; Fernandes et al. 2005; Panter et al. 2007) for a wide range of galaxy stellar masses ($10^7 - 10^{12} M_\odot$). Panter et al. (2007) found that stellar mass is the parameter that most directly determines the galaxy's star formation history and SED. Taking advantage of this finding, we use six mass ranges with their corresponding reconstructed star formation histories, to obtain six spectral templates. These templates should encompass the entire galaxy population and are therefore a representative basis of galaxies in the universe. The spectral templates are built using the input star formation history with solar metallicity (changing the template metallicity has little impact on the final photo- z performance) using the Bruzual & Charlot (2003) models. The models have only absorption lines, so for the star-bursting galaxy template (SED5 in Fig. 2) we use the emission lines from the Kinney et al. (1996) models and add them to this template only. The new templates – shown in Fig. 2 – provide a higher resolution and wider spectral range than other publicly available templates. Note that we have not adjusted the templates to obtain the best photometric redshifts, but rather we have used the physical knowledge of the recovered star formation history of the universe as our input. We evaluate the performance of these new templates below.

3.2. Template fitting photo- z calculation

With the addition of the two GALEX bands, our template-based methodology to obtain photo- z is fairly simple. We use the six galaxy templates in Fig. 2 and perform a maximum likelihood (ML) analysis, which is

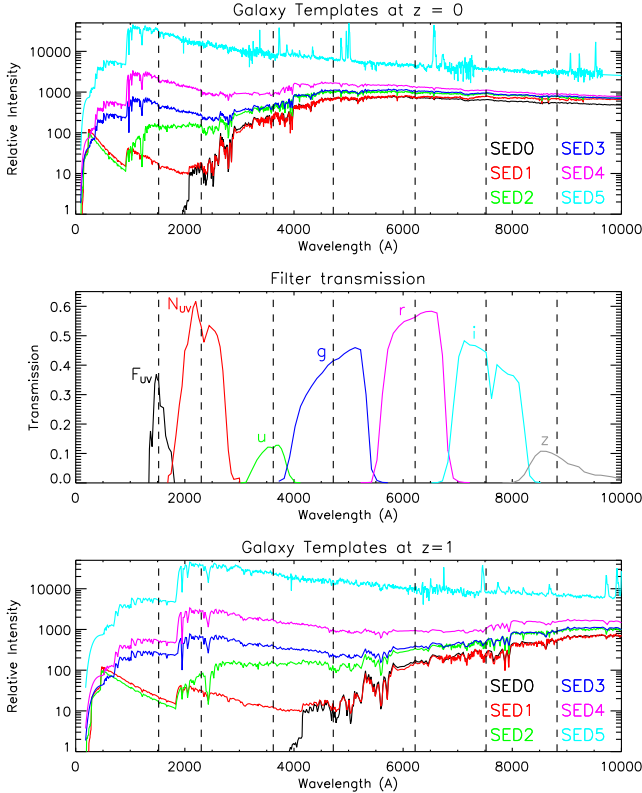


FIG. 2.— The top panel shows the six galaxy templates that are used to find the maximum likelihood solution for the photometric redshifts (§3.2). The vertical dashed lines show the central frequencies of the GALEX and SDSS bandpasses. The middle panel shows the two GALEX bands (F_{UV} , N_{UV}) as well as the five SDSS bands (u , g , r , i , z). The bottom panel shows the templates redshifted to $z = 1$. As the different galaxy types are redshifted, a redshift-brightness degeneracy arises in the optical bands (especially when only considering *griz* bands) for the galaxies with blue spectra. The addition of the GALEX bands breaks this degeneracy by sampling out to the 912 Å Lyman-limit. Note that by $z = 1$ the Lyman-limit has shifted out of the F_{UV} band, but it does not reach the central frequency of the more sensitive N_{UV} band until $z \approx 1.5$.

simply a chi-square minimization, to find the best fitting model to the observed photometry. No priors are used for this analysis, or more accurately, we assume flat redshift and template priors. We use two codes to compute the photo- z : BPZ¹⁶ (Benítez 2000) which has the ability to simultaneously calculate photo- z using both ML analysis and a Bayesian prior for comparison, and ZEBRA¹⁷ (Feldmann et al. 2006) which is a recently released independent code that uses similar techniques to BPZ. Most of our analysis will be done using BPZ because when including the *UV* data it performs significantly better than ZEBRA on our data set in the redshift range $0.25 < z < 0.4$; although, we note that slightly better results can be obtained by ZEBRA at $z < 0.25$.¹⁸

The observed magnitudes are matched to the predicted spectral energy distributions through each bandpass from the templates in Fig. 2. As suggested by

Benítez (2000), two points of interpolation are allowed between the different templates in color space, which allows the best fit template to be a (2:1 or 1:2) mix of two neighboring templates. The photo- z computation is set to have a precision of $\delta z = 0.01$. The only limit imposed in the ML calculation is a sharp prior $z < 1.5$; further, (as described above) we exclude from the sample the small number of sources with photo- $z > 1$.

3.3. Artificial neural-network photo- z calculation

We also consider the empirical photo- z method ANNz developed by Collister & Lahav (2004). We compare the performance of our template-based photo- z method to the results of Oyaizu et al. (2007), who trained and validated their artificial neural network on 640,000 galaxies with *ugriz* SDSS photometry and provide a photo- z catalog for SDSS galaxies with $r < 22$. We use their photo- z determinations for the galaxies in our sample as a benchmark to compare the performance of our template-based technique (§4.1 and Fig. 3, 4, 5, and 6). ANNz in this case yields a photo- z scatter of $\sigma_z = 0.027(1 + z)$.

To explore the photo- z potential of GALEX observations in more detail, we also use the publicly available ANNz code¹⁹ with our combined GALEX and SDSS catalog to obtain more accurate photo- z (henceforth ANNzG). We use as a training set the SDSS galaxies in our GALEX fields that also have spectra. Of the ~ 3000 objects with SDSS spectroscopic redshifts in our catalog 700 are used as our training set and 400 as our validation set. We then re-run ANNz on the full ~ 3000 objects to estimate its performance (§4.2). Two different network architectures were explored for the ANNzG analysis: one with five hidden layers with 10 nodes each and three committee members, and a simpler version with two hidden layers with 10 nodes each and no committee. The more complex architecture did result in a slight reduction of the photo- z scatter; however, the relative results of using different data combinations were nearly identical. We present the results of the simpler network analysis here. Note that all galaxies in the specified magnitude range are included in the ANNz and ANNzG analysis, since (unlike the template-based analysis) there are no galaxies with photo- $z > 1$, and because of the nature of the ANNz calculation, it can also simultaneously calculate the photo- z for the bluest objects, such as QSOs.

4. RESULTS

4.1. Photo- z analysis with no priors

The addition of GALEX data to the optical measurements alleviates the redshift-brightness degeneracy and greatly improves the photo- z estimation. In Fig. 3, the upper-left panel shows the ML recovered photo- z when using only *griz* data. As expected, the number of catastrophic failures is high, resulting in a large standard deviation of $\sigma_z = 0.17(1 + z)$. Addition of the *u* band data (upper-right panel) reduces the number of catastrophic failures and halves the standard deviation to $\sigma_z = 0.08(1 + z)$.²⁰ Including the GALEX data (middle panels) reduces the standard deviation to

¹⁶ Code version bpz.1.98b; acs.pha.jhu.edu/~txitxo/bpzdoc.html

¹⁷ www.exp-astro.phys.ethz.ch/ZEBRA/

¹⁸ The same differences between BPZ and ZEBRA were observed with a variety of galaxy templates when using the GALEX data; however, when the optical data is analyzed without GALEX data, BPZ and ZEBRA provide nearly identical results.

¹⁹ zuserver2.star.ucl.ac.uk/~lahav/annz.html

²⁰ We note that the standard deviation of the *ugriz* analysis is reduced by a 25% to $\sigma_z = 0.06(1 + z)$ if SDSS *model* magnitudes are used. These are the best internally calibrated magnitudes for SDSS

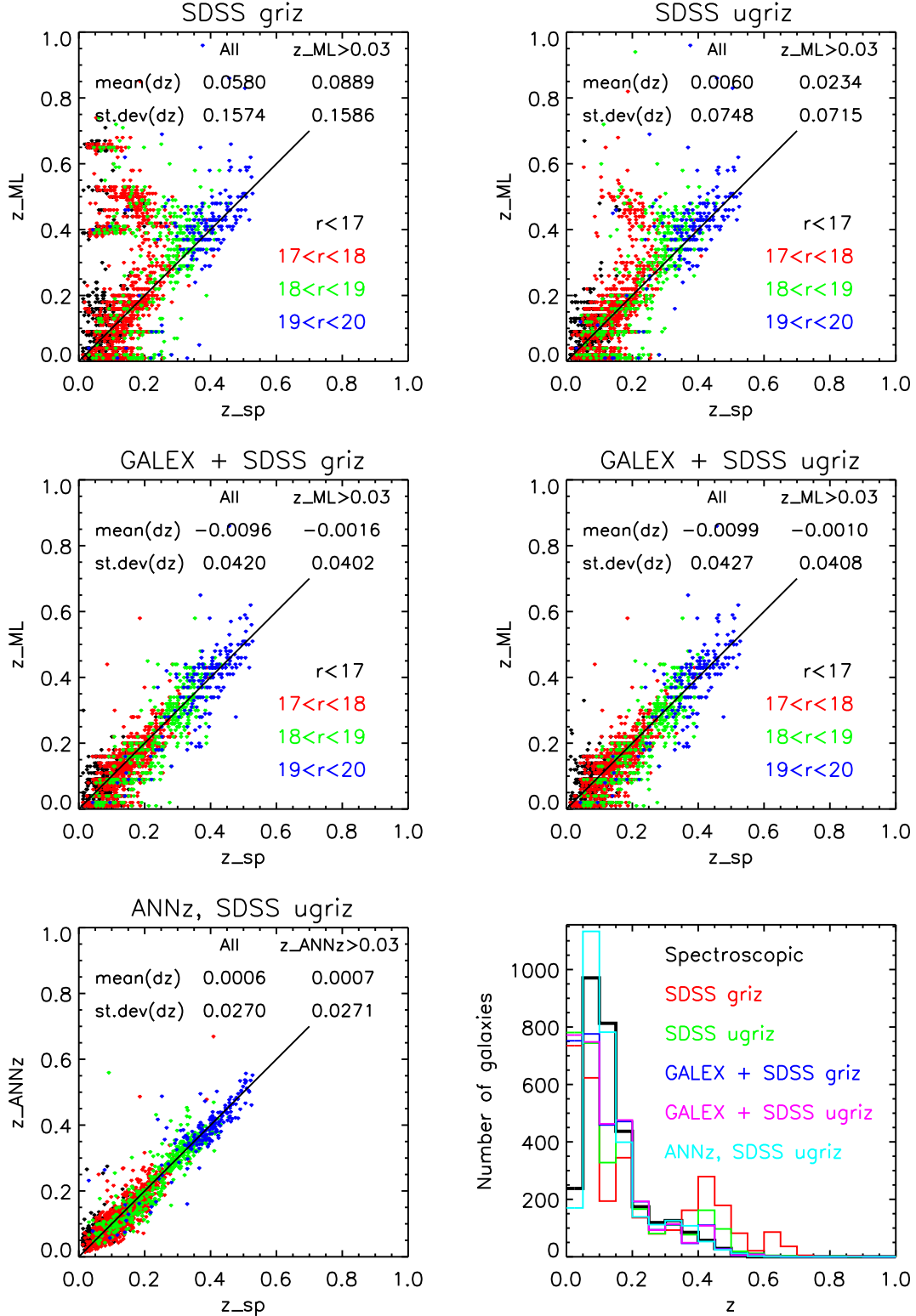


FIG. 3.— Comparison of our maximum likelihood photo- z redshift estimates (z_{ML}) and the ANNz estimates (z_{ANNz}) with SDSS spectroscopic measurements (z_{sp}). The colors on the five similar plots are different r magnitude bins. The top panels show photo- z estimates using only the optical *griz* (left) and *ugriz* (right) data. Adding the u -band data significantly improves the estimates, but in both analyses large groups of outliers exist in the $0.4 < z_{\text{ML}} < 0.6$ range. By adding the GALEX data (middle panels), this group of outliers is removed, and the photo- z predictions fall much closer to the spectroscopic measurements. Note that BPZ consistently results in an excess of galaxies in the lowest z bins, so the scatter and bias are quoted in the legends both for all galaxies and for those with photo- $z > 0.03$. In the lower left panel, we show the SDSS ANNz photo- z estimates for comparison. The ANNz technique does result in less scatter than adding the GALEX data; however, ANNz is being compared to a subset of its redshift training and validation set, as opposed to the ML analysis, which does not utilize any prior redshift information. The lower right panel compares the redshift distributions from the five photo- z analyses (colors) with the spectroscopic measurements (black).

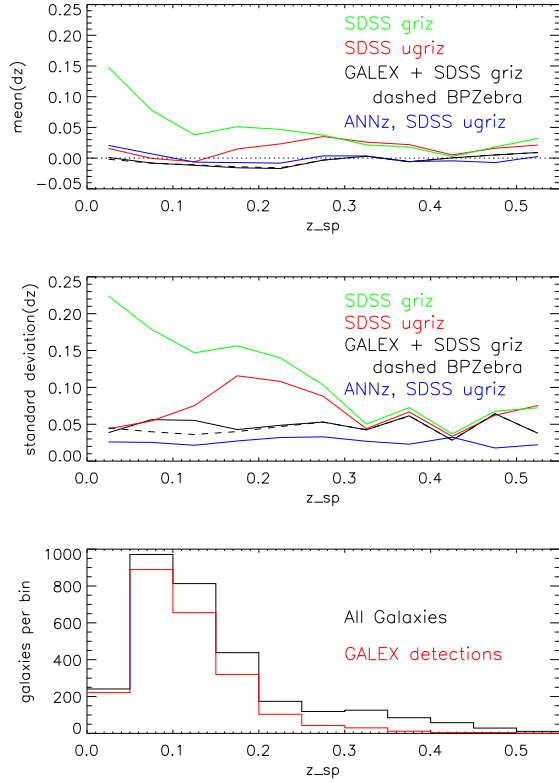


FIG. 4.— Errors in photo- z estimation versus spectroscopic redshift. The mean (top) and standard deviation (middle) of dz are shown as a function of redshift. We compare the ML photo- z results using the SDSS *griz* data (green), which is representative of the BCS measurements, as well as the SDSS *ugriz* data (red), the GALEX + *griz* data (black), and the SDSS ANNz results (blue). The GALEX + *griz* data approaches the standard deviation of the ANNz results without the use of priors or training sets. We also show the improvement that can be achieved in the GALEX + *griz* analysis by using the ZEBRA code for $z_{ph} < 0.25$ and BPZ code otherwise, which we call BPZebra (black dashed). In the bottom panel, the total number of sources in each z bin is shown (black) as well as the total number of sources with a GALEX detection (red).

$\sigma_z = 0.04(1+z)$ and removes nearly all catastrophic failures. Note that the addition of u data has negligible effect when the GALEX bands are added. The bottom-left panel shows the comparison with ANNz. The standard deviation of ANNz is $\sim 30\%$ smaller than GALEX + *griz*; although, we note that ANNz is being compared to a sample that includes its own training and validation set, which makes the comparison a bit unfair. We find that simply adding the GALEX moderate exposures to *griz* imaging and using ML analysis techniques with 6 empirically motivated galaxy templates provides photo- z approaching the accuracy of ANNz on *ugriz*.

We explore the performance of the photo- z in more detail in Fig. 4, 5, and 6 to investigate the dependence on redshift, magnitude, and color, respectively. In Fig. 4 we show how the photo- z bias and scatter evolve as a function of redshift. Adding the GALEX data dramatically reduces the bias and scatter over the optical bands alone at $z < 0.3$, beyond which the proportion of galaxies with GALEX detections falls off at the current GALEX observation depths (Fig. 4, bottom panel). Still, the performance approaches the level of ANNz up

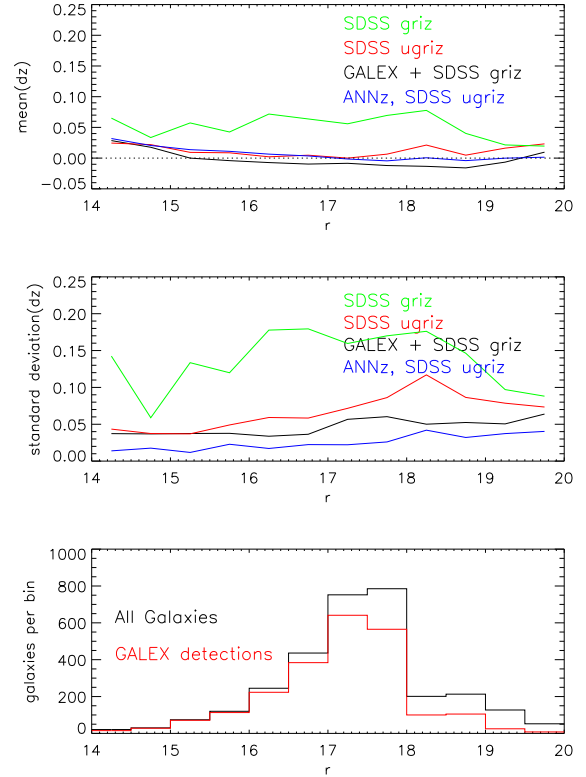


FIG. 5.— Errors in photo- z estimation versus source r magnitude. The mean (top) and standard deviation (middle) of dz are shown in different r bins. (Colors are the same as Fig. 4 and 6.) The GALEX + *griz* data approaches the standard deviation of the ANNz results without the use of priors or training sets. At the bottom, the total number of sources in each r bin is shown (black) as well as the total number of sources with a GALEX detection (red).

to near $z \approx 0.4$. In Fig. 5 we show the photo- z bias and scatter as a function of the source r magnitude. Both remain nearly flat in the regime $r < 19$, above which the fraction of galaxies detected by GALEX falls to less than $1/2$. These plots clearly indicate that with deeper GALEX exposures, we can expect to improve our results for fainter objects and higher redshifts. In Fig. 6 the photo- z performance as a function of galaxy color is examined. The scatter is equivalent to (or possibly even lower than) ANNz for $g-r < 0.6$ and is only slightly larger up to $g-r \approx 2$. When compared to the other ML methods without GALEX photometry, the addition of GALEX bands returns significantly more accurate photo- z for colors as red as $g-r = 1.4$.

We also consider removal of the excess of galaxies in the lowest BPZ redshift bins ($z < 0.03$). Cutting these galaxies results in a $\sim 5\%$ reduction of the standard deviation and almost a factor of ten reduction in bias (Fig 3, middle panels). At $z_{ph} < 0.25$ ZEBRA photo- z scatter is $\sim 8\%$ smaller than BPZ and does not show the excess in the lowest z bin. A hybrid technique (ZEBRA at $z_{ph} < 0.25$ and BPZ at $z_{ph} > 0.25$, which we call BPZebra) can be used to take advantage of the fact that ZEBRA does not have a pile-up of galaxies at low- z , which reduces the total scatter by $\sim 8\%$ and reduces the total bias by a similar amount to cutting the low- z galaxies (dashed line in Fig. 4).

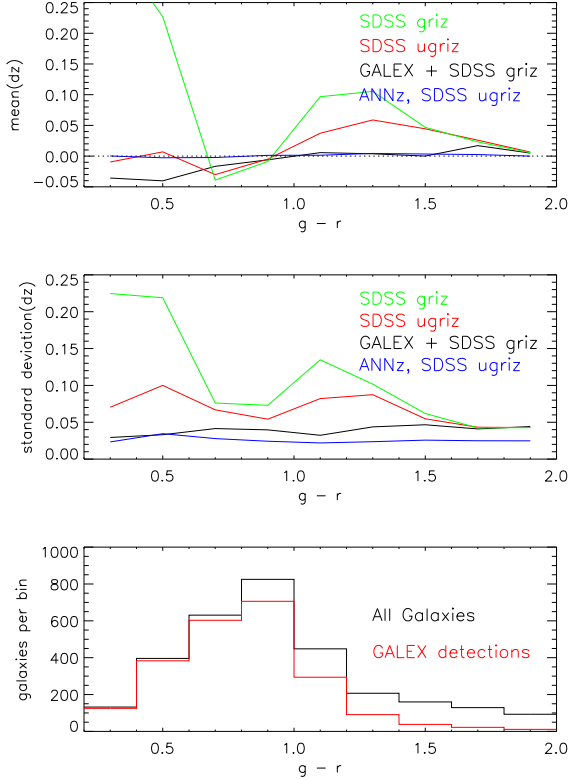


FIG. 6.— Errors in photo- z estimation versus color, $g-r$. The mean (top) and standard deviation (middle) of dz are shown in different $g-r$ bins. (Colors are the same as Fig. 4 and 5.) For the low $g-r$ bins, or blue galaxies, the standard deviation of the GALEX + $griz$ results are a huge improvement over the SDSS only data and are essentially equivalent to the ANNz results without the use of priors or training sets. At the bottom, the total number of sources in each $g-r$ bin is shown (black) as well as the total number of sources with a GALEX detection (red).

4.2. ANNz analysis for improving stripe 82 photo- z

The performance of ANNz using GALEX data (ANNzG, §3.3) is explored with several combinations of SDSS bands.²¹ The best performance is (not surprisingly) obtained with all five SDSS bands and GALEX (ANNzG: *ugriz*); in this case the scatter is $\sigma_z = 0.018(1+z)$. Removing the SDSS u (ANNzG: *griz*) or u and z (ANNzG: *gri*) bands only causes slight degradations in the photo- z scatters to $\sigma_z \approx 0.020(1+z)$. As a systematic test of our ANNzG approach, we run the same analysis on the SDSS *ugriz* data in our catalog and find that it gives $\sigma_z = 0.026(1+z)$, which is consistent with the scatter from the Oyaizu et al. (2007) ANNz pipeline on this data set of $\sigma_z \approx 0.027(1+z)$. These results combined with the results in §4.1 indicate that the GALEX bands provide superior redshift information to the SDSS u and/or z bands.

In Fig. 7 we explore the color, $g-r$, and magnitude, r , dependence of the photo- z scatter from the ANNzG and ANNz calculations. The addition of the GALEX data results in a clear and significant reduction in scatter for nearly all color and magnitude bins, with the exception of the reddest (high $g-r$) and brightest (low r) galaxies. The general consistency between trends in the ANNz

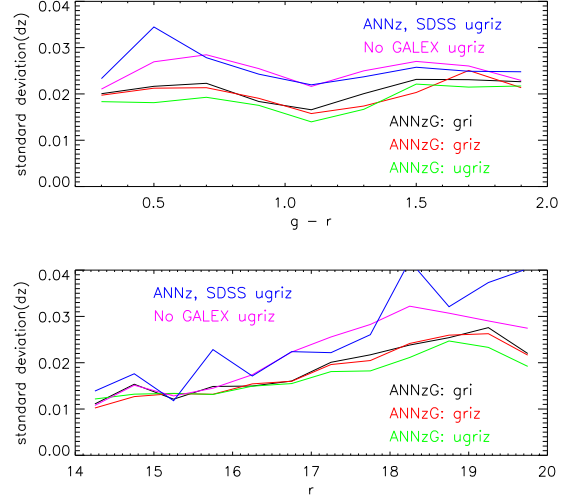


FIG. 7.— Artificial neural network photo- z scatter as a function of galaxy color, $g-r$ (top panel), and magnitude, r (bottom panel), analyzed as described in §3.3 for different combinations of SDSS and GALEX data. The scatter is compared to the performance of the Oyaizu et al. (2007) photo- z pipeline (ANNz, SDSS *ugriz*, blue) on the same data set. The addition of GALEX data to *ugriz* data (ANNzG: *ugriz*, green) provides the best photo- z predictions, while GALEX combined with *griz* (ANNzG: *griz*, red) and even just *gri* (ANNzG: *gri*, black) only results in slight increases in scatter compared to the complete data set. This indicates that the GALEX data provides more redshift information than the SDSS u or z bands. As a systematic check, we have run identical ANNz analysis on the SDSS *ugriz* data without GALEX (No GALEX *ugriz*, magenta), and we find that the scatter distribution is similar to that recovered by Oyaizu et al. (2007), both as a function of $g-r$ and r . The galaxy distributions in the scatter bins are those shown in the bottom panels of Fig. 5 and 6.

pipeline results (ANNz, SDSS *ugriz* in legend) and our own analysis applied to the SDSS only data (No GALEX *ugriz* in legend) is an indication that our ANNzG results are robust. The photo- z bias was also explored, and it was found to be roughly five to twenty times smaller than the scatter in each bin, so we do not discuss it further.

4.3. Public Photo- z Catalogs

Here we apply our ML (§3.2) and ANNzG (§3.3) approaches for calculating photo- z to stripe 82 galaxies that do not have spectroscopic data. The redshift distributions from these analyses as well as the SDSS ANNz pipeline are compared in Fig. 8. The top and bottom panels show the redshift distributions for galaxies with $r < 19$ and $r < 21$, respectively. Because of the lack of SDSS spectroscopic observations for GALEX detected galaxies with $r > 19$ (Fig. 5) and $z > 0.3$ (Fig. 4), the current ANNzG analysis does not have accurate training above this limit. The excess number of galaxies at $z \approx 0.3$ in the lower panel of Fig. 8 is due to the resulting failure of the ANNzG analysis for galaxies with $r > 19$. As expected, this clearly indicates that to use empirical photo- z techniques one must ensure that spectroscopic training sets are representative of the complete photometric sample.

The ML analysis, on the other hand, does not require spectroscopic training, and the lower panel of Fig. 8 shows that the ML analysis on galaxies detected by GALEX produces a similar distribution to the SDSS ANNz pipeline even for dimmer galaxies with $19 < r <$

²¹ We note that the training and validation sets are a random sub-sample of 36% of the catalog.

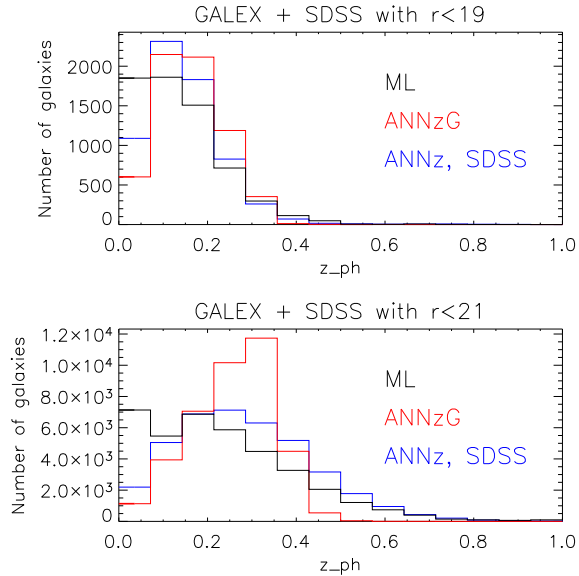


FIG. 8.— Comparison of photo- z distributions for SDSS data with GALEX detections. The top panel shows data with $r < 19$. The ML analysis (black), the ANNzG analysis (red), and the SDSS ANNz results (blue) are all relatively similar in this magnitude regime. The bottom panel compares the same three analyses on data with $r < 21$. The ANNzG analysis clearly fails here, because the current training set utilizes SDSS spectroscopic measurements, which have a lower magnitude distribution (Fig. 5, bottom panel). The ML analysis distribution has some failures as well, but it has significantly less bias than the ANNzG analysis. The excess in the lowest z bin has been observed in all ML analyses with GALEX data (Fig. 3). In our public catalogs, the ANNzG and ML results are provided for all galaxies with $r < 19$, while ML results are provided for all galaxies detected by GALEX with $r < 21$.

21. The primary difference between the ML and ANNz distributions is the excess in the ML lowest redshift bin, which is a known failure of the BPZ code used for this analysis (described in §4.1).

The resulting catalogs containing both the ML and ANNzG analyses for galaxies observed by GALEX will be made publicly available for the community at www.ice.csic.es/personal/jimenez/PHOTOZ. The catalogs will be updated with more complete versions as our GALEX stripe 82 observations are completed. Since the ANNzG analysis has only been trained up to $r \approx 19$, we provide an ANNzG photo- z catalog for all SDSS galaxies up to this limit as well as ML photo- z on those same galaxies. Since the ML analysis does not require spectroscopic training, we also provide a catalog with ML photo- z estimates for all SDSS galaxies that have GALEX detections and $r < 21$.

5. CONCLUSIONS

In order to obtain accurate photometric redshifts as efficiently as possible for the areas surveyed by SZ experiments, we have obtained moderate-depth GALEX photometry. With a modest observing campaign, and using already available MIS observations, we have already covered an area of $\sim 60 \text{ deg}^2$ to a mean depth of $\sim 3 \text{ ks}$. At the completion of our $\sim 210 \text{ ks}$ of observations, we will have covered $\sim 100 \text{ deg}^2$ to this depth.

Budavári et al. (2005) previously used *ugriz* SDSS DR1 photometry together with GALEX Medium Imaging Survey (MIS, 1.4 ks exposure) F_{UV} and N_{UV} photometry to determine photo- z for about 10000 galaxies

up to $z \approx 0.25$. They use an empirical technique which relies on a training set of about 6000 objects, and obtained photo- z errors of $\sigma_z = 0.026$ on the training set, which is similar to the SDSS ANNz performance. As large training sets and *u*-band data may not be available for the next generation large-area SZ cluster surveys and as *u*-band photometry may not be available for future optical surveys such as BCS, DES, and LSST, we have considered two cases.

To be independent of training sets, we considered a spectral-energy-distribution, or template-based, photo- z approach. As we have found that suitable templates for use with GALEX observations were not publicly available, we have constructed new, physically motivated, spectral templates. They are publicly available at www.ice.csic.es/personal/jimenez/PHOTOZ.

Using the SDSS spectroscopic survey we have shown that the addition of GALEX photometry to only *griz* bands makes possible the use of simple maximum likelihood techniques, without resorting to Bayesian priors. This approach obtains $\sigma_z = 0.04(1+z)$ for $r < 20$ galaxies, which includes luminous galaxies up to $z \approx 0.4$. This accuracy approaches that obtained using spectroscopic training of neural networks on *ugriz* photometry of the same galaxy sample. In particular, we have shown that the large number of catastrophic failures that occur for *griz*-based and *ugriz*-based maximum likelihood photo- z determinations is nearly eliminated by adding UV photometry from GALEX data to *griz* data. The improvement is especially notable for blue galaxies; for galaxies with $g - r < 0.6$, we obtain photo- z scatter of $\sim 0.03(1+z)$. We find that the addition of UV observations to *griz* photometry, provides significantly better photo- z than the addition of *u*-band observations.

Beyond $z \approx 0.4$, the GALEX $\sim 3 \text{ ks}$ exposures do not have a sufficient number of detections to dramatically improve the *griz* observations. Clearly, moderately deeper observations would help to bring the utility of GALEX observations closer to $z \approx 1$. We note that the current depth of $z \approx 0.4$ looks back through roughly 33% of the age of the universe and samples a volume of 15 Gpc^3 . Maybe more importantly, $\sim 20\%$ of the clusters that will be detected by the SZ experiments (above a dark matter mass of $3 \times 10^{14} M_\odot$) are at $z < 0.4$. If redshift up to $z = 1$ were accessible by GALEX, $\sim 60\%$ of the age of the universe and a volume of 153 Gpc^3 would be surveyed; 86% of the clusters that will be detected by the SZ experiments (above a dark matter mass of $3 \times 10^{14} M_\odot$) and 90% of the resolved ones, are expected to be at $z < 1$.

The most important aspect of the results presented here, is that the photo- z accuracy of $\sigma_z = 0.04(1+z)$ at $z < 0.4$ was obtained using only maximum-likelihood fits to six galaxy templates in BPZ, without resorting to priors or training-sets. As the acquisition of training sets or priors relies on obtaining large spectroscopic data-sets, we consider the moderate GALEX exposures an efficient way to obtain accurate photo- z over large areas.²² Further, GALEX photometry gives a direct measurement of

²² Note that we just integrated ~ 2.4 days and that, for example, a program 10 times longer could provide photo- z for about 1000 deg^2 , which (we estimate) is the optimal area to extract cosmological information from SZ surveys

star formation and AGN activity (Atlee & Gould 2007), a subject that we are continuing to explore.

Should large spectroscopic training sets be available, we have considered the effect of adding UV photometry to optical data on the performance of an artificial neural network photo- z calculation. The addition of GALEX observations to optical *griz* (or even just *gri*) observations yields photo- z that have $\sigma_z = 0.02(1+z)$, which is $\sim 30\%$ smaller scatter than was obtained on the same data set using only SDSS *ugriz* observations.

We make our photo- z catalogs of stripe 82 galaxies detected by GALEX publicly available at www.ice.csic.es/personal/jimenez/PHOTOZ. The catalogs contain the results of the ML photo- z calculation for all GALEX detected galaxies with $r < 21$ as well as the ANNzG and ML photo- z calculations for all SDSS stripe 82 galaxies in GALEX fields with $r < 19$. The posted catalogs will be updated as our GALEX observations and analysis are completed.

The approach proposed here can provide a useful catalog for weak-lensing studies as photo- z remain accurate for the bluest galaxies. These determinations are commonly the most difficult to obtain because spectra of blue galaxies in the optical bands show an almost featureless power law spectral energy distribution. We envision our SED-based ML approach to be useful for cross-correlation studies with CMB maps, where deep photo- z are needed over large areas and large training sets may not be available. Possible applications of these studies include improving our understanding of dark energy using cluster counting techniques (Carlstrom et al. 2005; Lima & Hu 2007), the kSZ effect (Hernández-Monteagudo et al. 2006), and the lensing of the CMB by large-scale structure (Carbone et al. 2007).

ACKNOWLEDGEMENTS

MN is grateful to Robert Lupton, John Hughes, Yen-Ting Lin, and Chris Hirata for their useful and informa-

tive discussions and suggestions as well as Peter Friedman for help with the GALEX data and his advisor, Suzanne Staggs, for supporting his work on this project. RJ and LV thank Txitxo Benítez for helpful discussions. The research of MN is supported by the U.S. National Science Foundation through grant PHY-0355328 as well as a Princeton University Centennial Fellowship. RJ acknowledges support from FP7-PEOPLE-2007-4-3-IRG grant and CSIC I3 grant 200750I037. LV acknowledges support of FP7-PEOPLE-2007-4-3-IRGn202182 and CSIC I3 grant 200750I034. RJ and LV are partially supported by GALEX grant GI3-095. RJ and DNS are partially supported by NSF grant PIRE-0507768.

Funding for the creation and distribution of the SDSS Archive has been provided by the Alfred P. Sloan Foundation, the Participating Institutions, the National Aeronautics and Space Administration, the National Science Foundation, the US Department of Energy, the Japanese Monbukagakusho, and the Max Planck Society. The SDSS Web site is www.sdss.org. The SDSS is managed by the Astrophysical Research Consortium (ARC) for the Participating Institutions. The Participating Institutions are the University of Chicago, Fermilab, the Institute for Advanced Study, the Japan Participation Group, The Johns Hopkins University, the Korean Scientist Group, Los Alamos National Laboratory, the Max Planck Institute for Astronomy (MPIA), the Max Planck Institute for Astrophysics (MPA), New Mexico State University, the University of Pittsburgh, Princeton University, the United States Naval Observatory, and the University of Washington.

The Galaxy Evolution Explorer (GALEX) is a NASA Small Explorer (www.galex.caltech.edu). The mission was developed in cooperation with the Centre National d'Etudes Spatiales of France and the Korean Ministry of Science and Technology.

REFERENCES

- Abazajian, K., et al. 2003, *Astron. J.*, 126:2081-2086.
 Agüeros, M., et al. 2005, *Astron. J.*, 130:1022-1036.
 Atlee, D. W., & Gould, A. 2007, *ApJ*, 664:53.
 Ball, N., et al. 2007, *ApJ*, 663:774.
 Baum, W. A. 1962, *Problems of Extra-Galactic Research*, 15, 390.
 Benítez, N. 2000, *ApJ*, 536:571.
 Benítez, N., et al. 2008, in preparation.
 Bertin, E., & Arnouts, S. 1996, *Astron. and Astrophys. Supp.*, 117:393.
 Bruzual, G., & Charlot, S. 2003, *MNRAS*, 344, 1000.
 Budavári, T., et al. 2005, *ApJLetters*, 61:L31.
 Carbone, C., Springel, V., Baccigalupi, C., Bartelmann, M., & Matarrese, S. 2007, *ArXiv Astroph. e-prints*, astro-ph/07112655.
 Carlstrom, J., et al. 2005, *Dark Energy Task Force white paper*.
 Coleman, G.D., Wu, C.-C., & Weedman D.W. 1980, *ApJS*, 43, 393.
 Connolly, A., et al. 1997, *ApJ*, 486:L11.
 Collister, A. A., & Lahav, O. 2004, *PASP*, 116, 345.
 Feldmann, R., et al. 2006, *MNRAS*, 372, 565.
 Fernandes, R. C., Mateus, A., Sodr , L., Stasińska, G., & Gomes, J. M. 2005, *MNRAS*, 358, 363.
 Heavens, A., Panter, B., Jimenez, R., & Dunlop, J. 2004, *Nature*, 428, 625.
 Hernández-Monteagudo, C., Verde, L., Jimenez, R., & Spergel, D. N. 2006, *ApJ*, 643:598.
 Ilbert, O., et al. 2006, *ArXiv Astroph. e-prints*, astro-ph/0603217.
 Kinney, A.L., Calzetti, D., Bohlin, R.C., McQuade, K., Storchi-Bergmann, T. & Schmitt, H.R. 1996, *ApJ*, 467:38.
 Koo, D. C. 1985, *AJ*, 90:418.
 Koo, D. C. 1999, *ASP Conf. Ser.*, 191, 3.
 Lima, M., & Hu, W. 2007, *Phys. Rev. D*, 76, 123013.
 Moles, M., et al. 2005, *ArXiv Astroph. e-prints*, astro-ph/0504545.
 Morrisey, P., et al. 2005, *ApJLetters*, 619:1, L7.
 Niemack, M. 2008, Ph. D. thesis, Princeton University.
 Oyaizu, H., Cunha, C., Lima, M., Lin, H., & Frieman, J. 2006, *Bulletin of the American Astronomical Society*, 38, 140.
 Oyaizu, H., Lima, M., Cunha, C. E., Lin, H., Frieman, J., & Sheldon, E. S. 2007, *ArXiv e-prints*, 708, arXiv:0708.0030.
 Padmanabhan, N., et al. 2007, *ArXiv e-prints*, 703, arXiv:0703.454v2.
 Panter, B., Jimenez, R., Heavens, A. F., & Charlot, S. 2007, *MNRAS*, 378, 1550.
 Sunyaev, R. A., & Zeldovich, Y. B. 1972, *Comm. Astroph. & Space Phys.*, 4, 173.
 Vanzella, E., et al. 2004, *A&A*, 423, 761.
 Way, M. J. & Srivastava, A. N. 2006, *ApJ*, 647:102.
 Wray, J. J., & Gunn, J. E. 2007, *ArXiv e-prints*, 707, arXiv:0707.3443. b